Electronic structure of metallic and insulating phases of vanadium dioxide and its oxide alloys

Haichang Lu,[1] Yuzheng Guo,[2] and John Robertson[1,*]

[1]*Department of Engineering, Cambridge University, Cambridge CB2 1PZ, United Kingdom*
[2]*School of Engineering, Swansea University, Swansea, SA1 8EN, United Kingdom*

VO$_2$ attracts much attention due to its metal-insulator transition. Alloying VO$_2$ with MgO and GeO$_2$ allows the band gap and the transition temperature to be varied. We find that the spin order plays a key role in creating the band gap in the low-temperature M_1 phase. For MgO alloying, the alloying fraction n (Mg$_n$V$_{1-n}$O$_{2-n}$) is varied from 12.5 to 33.3%. The minimum band gap does not change without a structural rearrangement because both band edges of insulating VO$_2$ consist of only V $3d$ states on sixfold-coordinated V sites. A crystal search finds that if the Mg fraction in the alloy is large enough ($>20\%$), fivefold-coordinated V sites can have lower energy than the sixfold sites, and the band gaps are doubled. For GeO$_2$ alloying, the insulating M_1 structure reverts to rutile because GeO$_2$ has a rutile phase. The result matches the experimental observation and is very important in guiding VO$_2$'s applications such as smart coating and nonlinear resistor.

I. INTRODUCTION

Pure vanadium dioxide (VO$_2$) has two phases; below 340 K it has the monoclinic or M_1 phase with a band gap, whereas above 340 K it has the metallic rutile form, called the *R* phase [1–3]. The phase transition is fully reversible so that it is a promising material for various applications [4] such as smart windows [5], optical [6] or rf switches [7,8], and as a component of steep slope transistors [9–11]. Although the structural change at 340 K has been heavily studied, the electronic structures and especially the magnetic ground states of both *R* and M_1 phases are still debated [1,3,12]. Experimentally, the magnetic order has been studied by NMR and electron paramagnetic resonance [12–15]. Theoretically, VO$_2$ is described as a strongly correlated system [16,17], as a Mott insulator with some Peierls character [18], but the relative importance of these two factors is debated [19]. There are disputes to what extent density-functional theory (DFT) can describe the two phases [1,20]. Here, we find that the antiferromagnetic order with a strong spin coupling between chains of vanadium dimers plays a major role in generating the gap, favoring a Mott description [21].

Apart from understanding the physics of pure VO$_2$, for applications it is of interest to vary the band gap of the insulating phase and vary the phase-transition temperature, while keeping the ability to switch between phases [22–24]. For instance, it is useful to shift the transition temperature T_C towards room temperature to enhance its suitability as a smart-window coating, or to raise the T_C to favor its use as a robust electrical or optical switch. It is also useful to be able to vary its optical gap for smart-window applications [5].

Experimentally, it is found that alloying VO$_2$ with MgO will widen its *p-d* band gap to 2.3 eV for alloying fraction $n = 19\%$ [22,23], whereas alloying VO$_2$ with GeO$_2$ will raise

its T_C [24]. However, so far there is little explanation of these effects in terms of electronic structure. Therefore, we carry out density-functional calculations of the electronic structure of pure and alloyed VO$_2$ to provide this.

We separate the dopants into those like Cr or Nb which will dope VO$_2$ in a substitutional fashion [2], where they change the *d*-electron count, to elements like Ge which behave like network-forming elements (in glass science) which alter the network bonding, to elements like Mg that behave like network modifiers which lower the coordination of the network.

It is interesting to compare alloying in *d*-electron systems like VO$_2$ to *s*, *p* bonded alloys like GaAs–AlAs whose band edges roughly interpolate between the energies of their end members. In VO$_2$ alloys, the band-edge states are always formed from V $3d$ states. For these, the number of occupied V $3d$ states may change, but the band gap is controlled by the V-V dimerization effect and spin coupling. As the band gap is determined mainly by the dimer itself, the magnitude of the band gap hardly changes, unless there is a change in the coordination of the V sites; in other words, it only varies by the action of the network-modifying elements.

II. METHODS

The calculation method is an important factor in the study of the alloys. The simple DFT method does not give a band gap for the M_1 phase [1]. In contrast, the more expensive methods such as GW or dynamic mean-field theory will reproduce the full electronic structure features [3] but are too computationally expensive for our case, given the need to use the large unit cells to treat dilute alloys.

Eyert [1,20] noted that moderate cost methods such as hybrid functionals, which add a fraction of nonlocal (Hartree-Fock) exchange to the DFT local exchange-correlation function, can give a reasonable, bandlike description of the electronic states. Rubio and co-workers [25] noted that it is the inclusion of nonlocal exchange rather than strong correlations
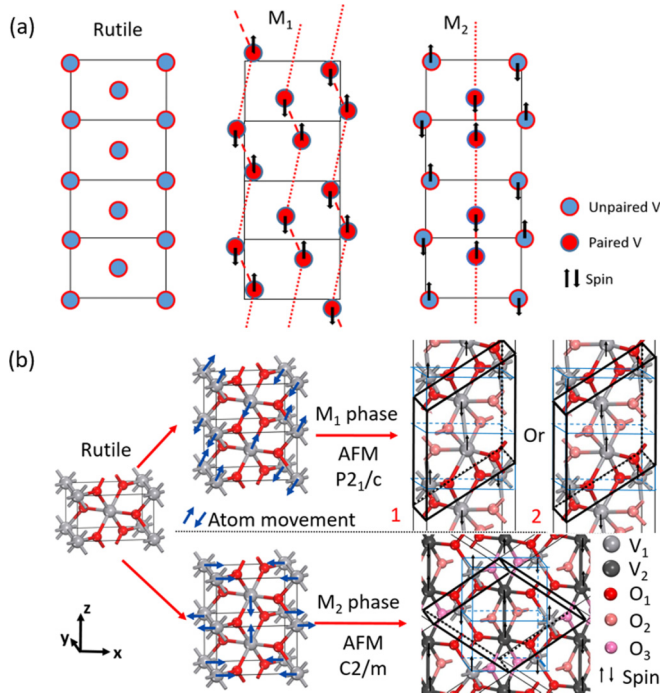
*jr214@cam.ac.uk

FIG. 1. (a) How the V sites spin pair as dimers and chains. (b) Structural transition from rutile phase to M_1 (up half) and M_2 (down half) phases via doubling the primitive rutile cell in z axis. The blue arrows indicate how the V atoms shall move while the black arrow is the spin direction. The thin black lattice is the $1 \times 1 \times 2$ rutile lattice while the thick black lattice is the monoclinic lattice of M_1 and M_2.

which is the key factor to cure the local density approximation band-gap error for these oxides.

Eyert [20] used the Heyd-Scuseria-Ernzerhof hybrid functional [26] with the standard mixing fraction of $\alpha = 0.25$. However, this gave a band gap larger than the experimental value of 0.6 eV [21,27–29]. Schwingenschlögl and coworkers [30] noted that hybrid functionals with $\alpha = 0.25$ give incorrect magnetic ground-state energies for both phases. Franchini [31] noted that hybrid functionals should use a lower value than $\alpha = 0.25$ for such correlated oxide perovskites. Similarly, Pantelides and co-workers [32] noted that hybrid functionals with a lower fraction of $\alpha \sim 0.1$ would work for VO_2. Recently, Zunger and co-workers [33] noted that allowing low-symmetry spin and structural states was a critical factor in the appearance of a band gap for related

perovskite metal oxides, even when using relatively simple density-functional methods.

Our analysis finds the spin pairing in V-V dimers is critical to opening up gaps. As regards whether VO_2 is a Mott-Hubbard or Peierls insulator, Huffman [21] noted that this corresponds in the Hubbard Hamiltonian to whether U or the hopping term t is dominant. It corresponds to whether the dimers are in the valence bond or molecular orbital limit. The role of fast lattice relaxations is seen in time-resolved studies [34,35].

Our calculations were carried out using the CASTEP plane-wave density-functional code [36]. It has been noted that the GGA + U method will give similar results to hybrid functionals for these open-shell metal oxides, so we use the GGA + U method to study the atomic and electronic structure of the alloys. The Perdew-Burke-Ernzerhof form of generalized gradient approximation (GGA), including an onsite repulsive potential U for V 3d electrons was used. Values of U from 2 to 3.25 eV were tested and finally $U = 2.5$ eV was used. Ultrasoft pseudopotentials with a plane-wave cutoff energy of 340 eV are used. The geometry optimization algorithm is the two-point steepest descent for an initial rapid search of atomic structure, followed by the Broyden-Fletcher-Goldfarb-Shanno method for accurate structure calculation [36]. The relaxation is performed until the residue force is less than 0.03 eV/Å. The density of k-point sampling varies for different cell size and is given in the Results and Discussion section. All calculations are spin polarized but spin-orbit coupling is excluded.

III. RESULTS AND DISCUSSION

A. Pure VO_2: From rutile to M_1 and M_2 phase

Firstly, we study how the insulating phases are derived from the rutile phase. We calculated structure, magnetic order, and partial density of states (PDOS) of each phase. There are two monoclinic phases M_1 and M_2.

The M_1 and M_2 phase together with the T phase differ in the fraction of V sites that are dimerized, and how any dimers are arranged into chains, Fig. 1(a). In rutile $P4_2/mnm$, the metal-oxygen distances are equal. In M_1, all dimers form into a single type of chains along the z axis of the rutile lattice. In M_2, half of the dimers make chains; half of the V sites are undimerized. The T phase is intermediate between $M1$ and $M2$. Figure 1(b) shows how the monoclinic phases are formed from $1 \times 1 \times 2$ of primitive cells of the rutile phase.

TABLE I. Calculated lattice constant of various VO_2 phase compared with previous work. Note that for M_2 the lattice constant of the conventional cell rather than the primitive cell is shown to compare to other papers.

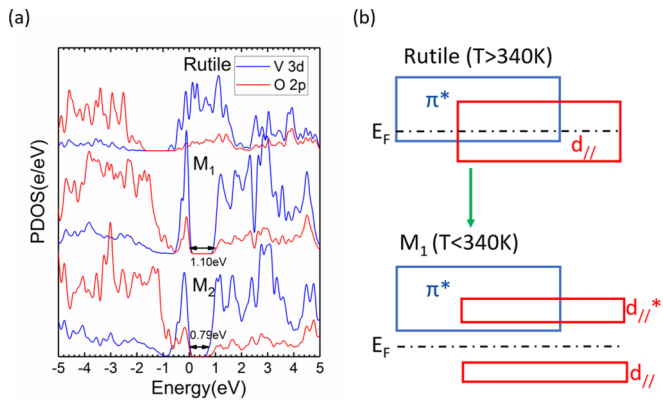| Lattice constant (Å)	Rutile		M_1		M_2	
	This work	Ref. [1]	This work	Ref. [1]	This work	Ref. [1]
a	4.62	4.55	5.67	5.75	9.05	9.06
b	4.62	4.55	4.61	4.54	6.03	5.80
c	2.78	2.85	5.44	5.38	4.52	4.52
α	90.00	90.00	90.00	90.00	90.00	90.00
β	90.00	90.00	122.13	122.65	90.50	91.85
γ	90.00	90.00	90.00	90.00	90.00	90.00

FIG. 2. (a) PDOS) of rutile, M_1, and M_2 phases. (b) Schematic band diagram of the metal-insulator transition [2].

The structures and cells of R, M_1, and M_2 are relaxed and the lattice constants of each phase are given in Table I with comparison to other papers. A $3 \times 3 \times 3$ k point is used for the PDOS calculation shown in Fig. 2(a). The opening and closing of band gaps during metal-insulator transition are often attributed to a structural change. However, the gap is mainly induced by the spin pairing along the V chains which splits the $d_{//}$ states as shown in Fig. 2(b). This follows because a gap exists in the rutile structure if it has antiferromagnetic (AFM) order, (unlike experimentally). On the other hand, a nonmagnetic monoclinic phase is gapless.

We find the ground state of monoclinic insulating phases should be AFM, where the chains of vanadium atoms have the opposite spin directions. In M_1, there are two spin configurations as in Fig. 1(b). Configuration 1 is that adjacent chains have the same spin orders while configuration 2 is that adjacent chains have opposite spin orders. While one can

further make larger supercells and create more AFM configurations, this is unnecessary because the energy difference between configuration 1 and 2 is negligible and the difference of electronic structures are also negligible. In M_2, there is only one spin configuration shown in Fig. 1(a).

There is strong spin coupling between two chains of V atoms with opposite spin, while the two adjacent V atoms with the same spin direction are weakly coupled. We think the strength of spin coupling which is the distance between the V atoms with opposite spin is the key to determine the band gap. In M_1, all vanadium atoms lie in chains and strongly coupled with another V so a band gap of 1.10 eV is calculated. In M_2, only 50% of V sites are in chains and strongly coupled; therefore, the band gap is calculated to be 0.79 eV. In rutile, no V atom is spin coupled; therefore, it is gapless. The PDOSs are shown in Fig. 2(a). Apart from the band gap, there should be a small gap in M_1 and M_2 phase which isolates the d bands in the valence-band maximum (VBM) and O 2p bands, as Eyert [1] argues.

For each V-V chain, there is one d band in the valence band (VB) known as $d_{//}$ because the orbital is parallel to the chain direction, and nine d bands in the conduction band (CB) which consist of both $d_{//}^*$ and π^*. These results are consistent with Goodenough's model [2]. If the temperature is close to T_C, the energy difference between the M_1 and M_2 phase should be very small because the spin order is going to disappear. Apart from M_1 and M_2, the triclinic T phase occurs as the intermediate phase between M_1 and M_2. The T phase does not appear in our oxide alloys.

B. MgO alloying of low-temperature monoclinic structures

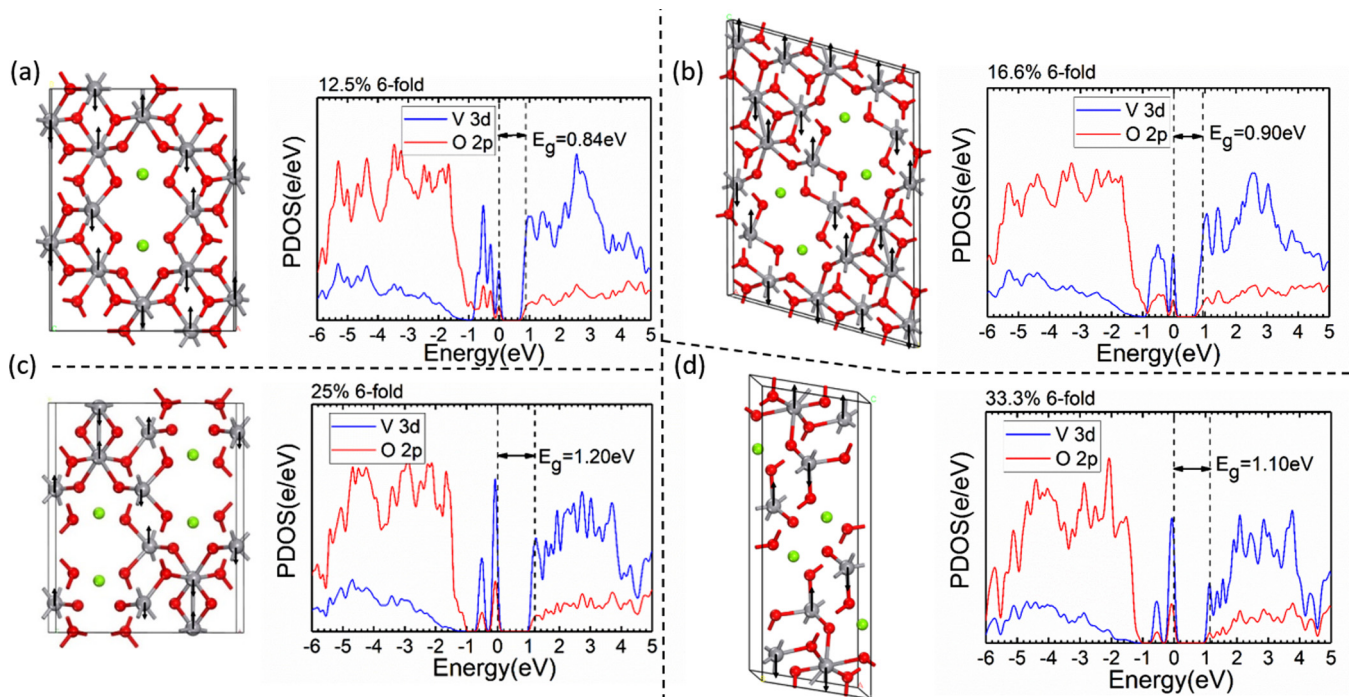It is found experimentally that MgO doping can raise VO$_2$'s p-d band gap to at least 2.32 eV as the ratio is 19%

FIG. 3. Structure; spin configuration and PDOS of (a) 12.5%, (b) 16.6%, (c) 25%, (d) 33.3% MgO alloying VO$_2$, sixfold.

[22,23]. Other dopants like Al, Fe, Si have been tried, but there is no increase in the band gap [37]. Unlike them, MgO is highly ionic with a large band gap of 7.4 eV, and it has no state near Fermi level in the alloys. The lattice constant can be increased due to the larger spatial separation of Mg and O. In this work, we choose alloying ratios of 12.5, 16.6, 25, and 33% for both M_1 and M_2 phase, as this creates supercell with a substitution ratios of 1:7, 1:5, 1:3, 1:2. One can either choose to substitute each V with Mg and delete one oxygen, or insert MgO into the supercell and do a geometry relaxation. These are the same and we choose the first method to help us obtain symmetric initial structures. We use a $1 \times 1 \times 3$ k-point mesh.

The relaxed structures of MgO alloys are shown in Figs. 3(a)–3(d). We find that irrespective of how M_1 or M_2 is alloyed, the final structures are the same and have nearly 50% of V dimer chains, which is M_2-like, maintaining sixfold-coordinated V sites. Figure 3 shows the relaxed structures, spin order, and PDOS of the alloys with 12.5, 16.6, 25, and 33% of MgO. We choose the initial centrosymmetric structures so that they can better comply with AFM. We do not break the V-V chains as this would create V dangling bonds, so a 2-Mg unit is necessary. Furthermore, we distribute the 2-Mg units evenly in the supercell. We find all the alloys are AFM and with the V site sixfold, which means these structures form one of the energy minima. However, they are only one of the metastable states for $n > 20\%$. These structures are not necessarily the only alloying configurations for each ratio, but we find different configurations with centrosymmetry have similar electronic structures and their energy differences are negligible. We can see V $3d$ bands in the VBM split due to the lowering of symmetry. The ratio of occupied and unoccupied d bands is still 1:9. Figure 4(a) shows the trend of the ratio of V-V chains and the densities of alloys. Figure 4(b) shows the trend of the band gap. As n increases, the V-V chain ratio decreases, the density decreases, and the band gap increases, by a small range. We find that unless the V–O bonding changes, there is no significant change in the gap. This is inconsistent with experiment, so the sixfold structures energies are no longer the global minima. Figure 4(c) shows the difference in phase energy per VO$_2$ formula unit.

As n increases above 20%, the structures undergo rearrangement. The Mg–O bond is ionic and nondirectional, so the supercell can adopt the lowest energy. From crystal structure searches [38] we find that a lower energy with AFM exists. The energy differences per formula unit are shown in Fig. 4(c), stating that the new "fivefold structures" energies are ∼0.5 eV per formula unit lower than their sixfold counterparts. Figures 5(a), 5(c), and 5(e) shows three fivefold cubic structures and spin orders with $n = 20$, 25, and 33.3%. The symmetries increase from $P2$ to $P4/n$, P_{nma}, and C_{mcm}, respectively. The PDOS are also shown in Figs. 5(b), 5(d), and 5(f). The reconstruction helps Mg distribute more evenly among the supercell and Mg is no longer dimerized. The average spatial separation between V sites of opposite spin is smaller than for sixfold structures, so the spin coupling is increased. Figure 5(b) shows that the band gaps are nearly twice as large as the sixfold sites.

We also calculate the PDOS of the nonmagnetic fivefold structures in Figs. 4(b), 4(d), and 4(f), corresponding to high-temperature cases. We keep the structure while eliminating the
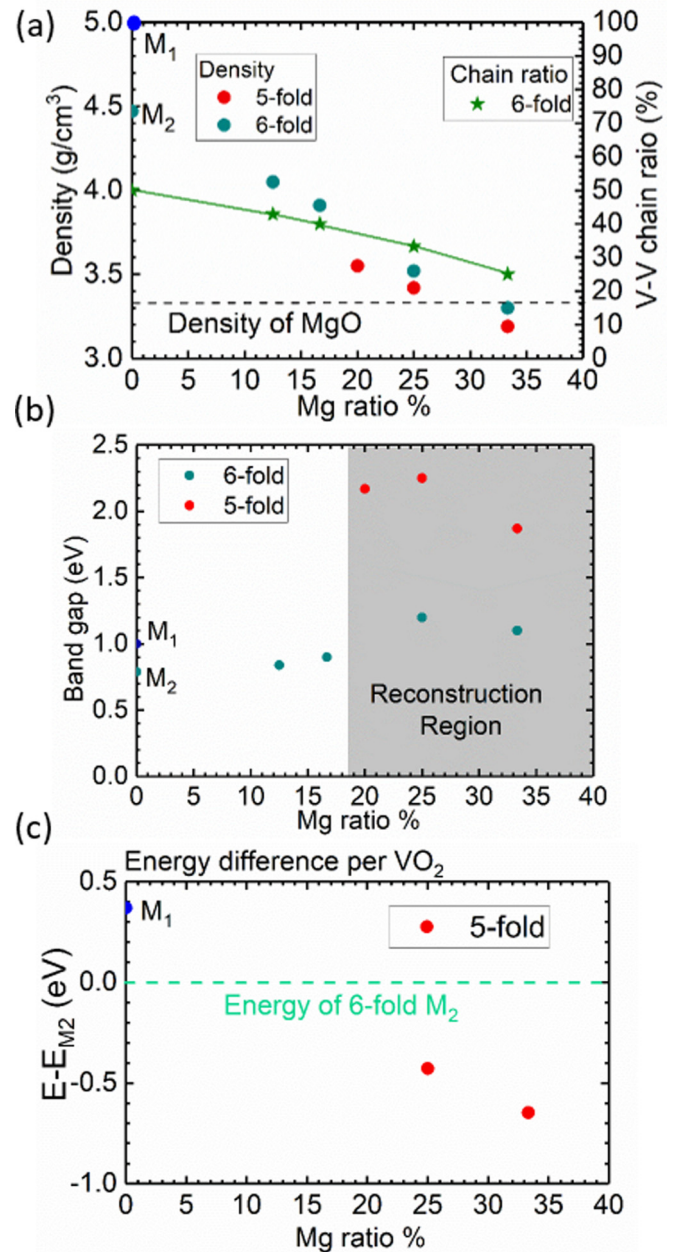

FIG. 4. (a) Density of alloys, V-V chain ratio vs the MgO ratio. (b) The band gap vs the MgO ratio. (c) The energy difference of sixfold (M1) and fivefold MgO alloys per formula unit.

spin because the structural transition is negligible compared to magnetic order change. We find that as the spin disappears, the gap also disappears. Therefore, we note that the fivefold structures are potentially useful for phase-switch applications.

C. GeO$_2$ alloying

We have also calculated the case of alloying VO$_2$ with tetravalent Ge. A 25% GeO$_2$ alloy (GeV$_3$O$_8$) is shown in Fig. 6. We initialize with AFM ordering and find that AFM is maintained during relaxation and a gap of 0.78 eV is obtained. Unlike MgO, the alloy structure reverts from M_1 to rutile structure, as shown in Figs. 6(c) and 6(d), where the
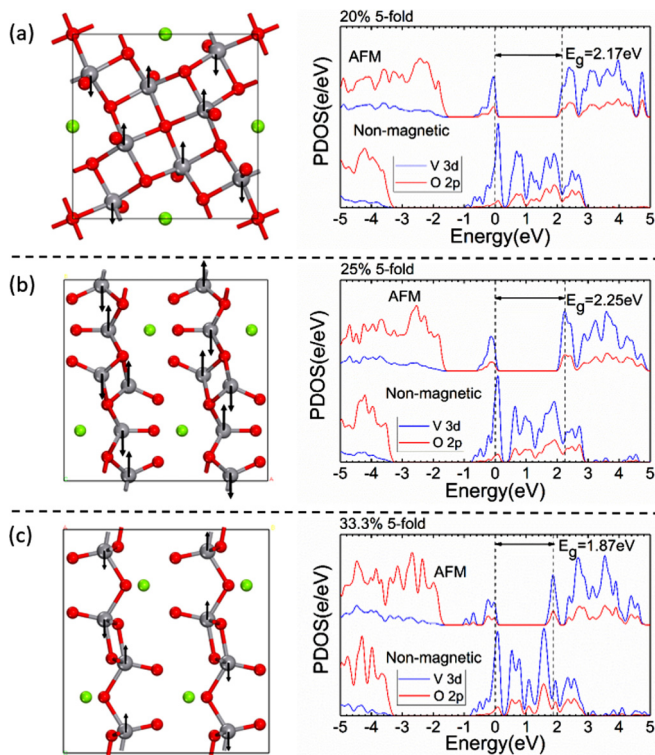
FIG. 5. Structure; spin configuration and PDOS of (a) 20%, (b) 25%, (c) 33% MgO alloying VO_2, with fivefold V sites.

side view shows that the M_1-type deformation disappears as Ge is doped. This is because GeO_2 has a metastable rutile phase which allows the alloy to revert to rutile. However, the spin order, as shown previously, is relatively independent of structural order. If the temperature is low enough, the first-order symmetry breaking will happen. Therefore, AFM is still
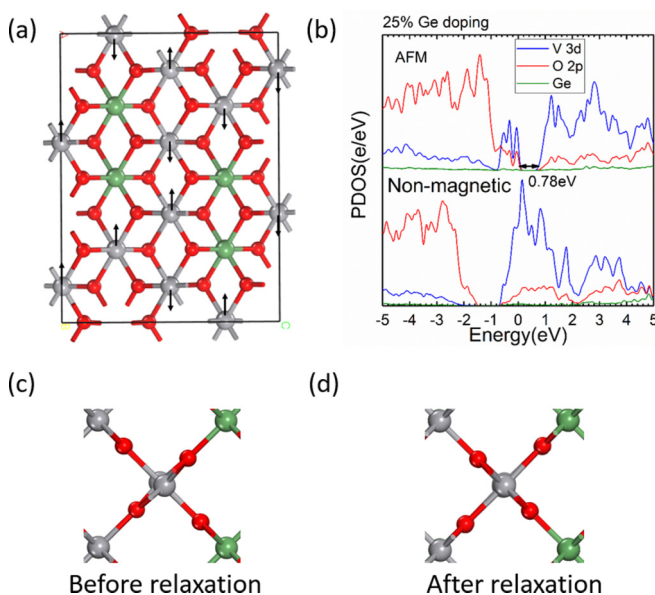

FIG. 6. (a) Structure, spin order and (b) PDOS of 25% GeO_2-VO_2 alloying. (c) Before and (d) after the geometric relaxation to show that the structure returns to rutile form.

maintained in a low-temperature phase. We then predict that by controlling the amount of Ge doping, we can control the phase-change temperature. A calculation of the total energy with the nonmagnetic and AFM spin ordering finds that the energy difference between the metallic and nonmetallic phases increases, equivalent to a rise in transition temperature from 340 to 373 K for 25% Ge, as observed experimentally [24].

Figure 6(a) shows the spin ordering for the VO_2:GeO_2 alloy. Unlike the insulating phase of pure VO_2, spin pairing along the z axis occurs without any structural pairing of V-V sites. The structure here assumes Ge atoms lie on one of the two chains. The spin pairing is weakened by the overall spatial separation of V, thus reducing the gap to 0.78 eV. Krammer *et al.* [24] show that the transition temperature can be raised by Ge doping, indicating the magnetic ground-state energy is lower.

The transition temperature T_c depends linearly on the total energy difference per formula unit between the metallic and insulating phases. This increase in energy difference raises T_c for GeO_2 alloying, which will be covered in detail elsewhere. An increase is consistent with experiment [24].

Generally, the spin alignment depends on the location of the dopant atoms within the chains of V sites, so that the V sites can pair up antiferromagnetically. However, the V pairing is able to occur for various spatial orderings of the dopant atoms. Thus VO_2 (unlike V_2O_3) is not so sensitive to disorder, as noted both experimentally or theoretically [18,39].

IV. CONCLUSION

We have calculated the structure and electronic structure of pure VO_2 and MgO, GeO_2 alloying VO_2. We found that the spin order, which is AFM, is more important than structural change for the creation of the band gap. The spin coupling between chained V sites is crucial.

By alloying MgO, we find a structural rearrangement happens as a high fraction of MgO is added, which causes the dramatic increase of the bonding and the band gap. This result is different from the previous view that Mg is a dopant. We emphasize that additives like MgO are unlike other dopants as MgO is highly ionic so it does not affect the electronic structure directly, but changes the bonding via encouraging structural reconstruction. Therefore, no midgap state is presented.

By substitutional doping with Ge, which is same as GeO_2 alloying, the insulating phase is returned to rutile, although the AFM and the gap are preserved because GeO_2 is rutile.

This work provides a detailed structure and magnetic order study of VO_2 and its metal-oxide alloying to explain the experimental observation.

[1] V. Eyert, Ann. Phys. (Leipzig) **11**, 9 (2002).

[2] J. B. Goodenough, J. Solid State Chem. **3**, 490 (1971).

[3] K. Liu, S. Lee, S. Yang, O. Delaire, and J. Wu, Mater. Today **21**, 875 (2018).

[4] Z. Yang, C. Y. Ko, and S. Ramanathan, Ann. Rev. Mater. Res. **41**, 337 (2011).

[5] S. Wang, M. Liu, L. Kong, Y. Long, X. Jiang, and A. Yu, Prog. Mater. Sci. **81**, 1 (2016).

[6] P. Markov, R. E. Marvel, H. J. Conley, K. J. Miller, R. F. Haglund, Jr., and S. M. Weiss, ACS Photonics **2**, 1175 (2015).

[7] W. A. Vitale, L. Petit, C. F. Moldovan, M. Fernandez, A. Paone, A. Schuler, and A. M. Ionescu, Sens. Actuators A **241**, 245 (2016).

[8] E. A. Casu, N. Oliva, M. Cavalieri, A. A. Muller, A. Fumarola, W. A. Vitale, A. Krammer, A. Schuler, M. Fernandez, and A. M. Ionescu, IEEE J. EDS **6**, 965 (2018).

[9] N. Shukla, A. V. Thathachary, A. Agrawal, H. Paik, A. Aziz, D. G. Schlom, S. K. Gupta, R. Engel-Herbert, and S. Datta, Nat. Commun. **6**, 7812 (2015).

[10] T. Yajima, T. Nishimura, and A. Toriumi, Nat. Commun. **6**, 10104 (2015).

[11] W. A. Vitale, E. A. Casu, A. Biswas, T. Rosca, C. Alper, A. Krammer, G. V. Luong, O. T. Zhao, S. Mantl, A. Schuler, and A. M. Ionescu, Sci. Rep. **7**, 355 (2017).

[12] A. X. Gray *et al.*, Phys. Rev. Lett. **116**, 116403 (2016).

[13] J. P. Pouget, H. Launois, T. M. Rice, P. Dernier, A. Gossard, G. Villeneuve, and P. Hagenmuller, Phys. Rev. B **10**, 1801 (1974).

[14] J. P. d'Haenens, D. Kaplan, and P. Merenda, J. Phys. C **8**, 2267 (1975); F. Chudnovskii and G. Stefanovich, J. Solid State Chem. **98**, 137 (1992).

[15] S. K. Misra, S. I. Andronenko, and R. Andronenko, Phys. Rev. B **57**, 8203 (1998).

[16] S. Biermann, A. Poteryaev, A. I. Lichtenstein, and A. Georges, Phys. Rev. Lett. **94**, 026404 (2005).

[17] M. Gatti, F. Bruneval, V. Olevano, and L. Reining, Phys. Rev. Lett. **99**, 266402 (2007).

[18] C. Weber, D. D. O'Regan, N. D. M. Hine, M. C. Payne, G. Kotliar, and P. B. Littlewood, Phys. Rev. Lett. **108**, 256402 (2012).

[19] H. Zheng and L. K. Wagner, Phys. Rev. Lett. **114**, 176401 (2015).

[20] V. Eyert, Phys. Rev. Lett. **107**, 016401 (2011).

[21] T. J. Huffman, C. Hendriks, E. J. Walter, J. Yoon, H. Ju, R. Smith, G. L. Carr, H. Krakauer, and M. M. Qazilbash, Phys. Rev. B **95**, 075125 (2017).

[22] S. Hu, S. Li, R. Ahuja, C. G. Granqvist, K. Hermansson, G. A. Niklasson, and R. H. Scheicher, Appl. Phys. Lett. **101**, 201902 (2012).

[23] S. Li, N. R. Mlyuka, D. Primetzhofer, A. Hallén, G. Possnert, G. A. Niklasson, and C. G. Granqvist, Appl. Phys. Lett. **103**, 161907 (2013).

[24] A. Krammer, A. Magrez, W. A. Vitale, P. Mocny, P. Jeanneret, E. Guibert, H. J. Whitlow, A. M. Ionescu, and A. Schüler, J. Appl. Phys. **122**, 045304 (2017).

[25] F. Iori, M. Gatti, and A. Rubio, Phys. Rev. B. **85**, 115129 (2012).

[26] J. Heyd, G. E. Scuseria, and M. Ernzerhof, J. Chem. Phys. **118**, 8207 (2003).

[27] L. A. Ladd and W. Paul, Solid State Commun. **7**, 425 (1969).

[28] T. Koethe, Z. Hu, M. Haverkort, C. Schlusser, F. Venturini, N. B. Brookes, O. Tjernberg, W. Reichelt, H. H. Hsieh, H. J. Lin, C. Chen, and L. Tjeng, Phys. Rev. Lett. **97**, 116402 (2006).

[29] S. Lee, T. L. Meyer, C. Sohn, D. Lee, J. Nichols, D. Lee, S. S. A. Seo, J. W. Freeland, T. W. Noh, and H. N. Lee, APL Mater. **3**, 126109 (2015).

[30] R. Grau-Crespo, H. Wang, and U. Schwingenschlögl, Phys. Rev. B **86**, 081101(R) (2012).

[31] C. Franchini, J. Phys.: Condens. Matter **26**, 253202 (2014).

[32] S. Xu, X. Shen, K. A. Hallman, R. F. Haglund, and S. T. Pantelides, Phys. Rev. B **95**, 125105 (2017).

[33] J. Varignon, M. Bibes, and A. Zunger, Nat. Commun. **10**, 1658 (2019).

[34] A. Cavalleri, T. Dekorsy, H. H. W. Chong, J. C. Kieffer, and R. W. Schoenlein, Phys. Rev. B **70**, 161102(R) (2004).

[35] S. Wall *et al.*, Science **362**, 572 (2018).

[36] S. J. Clark, M. D. Segall, C. J. Pickard, P. J. Hasnip, M. J. Probert, K. Refson, and M. C. Payne, Z. Kristallogr. **220**, 567 (2005).

[37] Q. Ren, Y. Cai, and Y. Gao, Comput. Mater. Sci. **150**, 337 (2013).

[38] A. Jain *et al.*, APL Mater. **1**, 011002 (2013).

[39] J. G. Ramirez, T. Saerbeck, S. Wang, J. Trastoy, M. Malnou, J. Lesueur, J.-P. Crocombette, J. E. Villegas, and I. K. Schuller, Phys. Rev. B **91**, 205123 (2015).